Electrospun black titania nanofibres: Influence of hydrogen plasma induced disorder on the electronic structure and photoelectrochemical performance

A. Lepcha, [a] *C. Maccato,* [b] *A. Mettenbörger,* [a] *T. Andreu,* [c] *, L. Mayrhofer,* [d] *M. Walter,* [d]

S. Olthof, [e] *T.-P. Ruoko,* [a,g] *A.Klein,* [a] *M. Moseler,* [d] *K. Meerholz,* [e] *J.R. Morante,* [c] *D. Barreca,* [f]

S. Mathur. [†,*]

[a] *Institute of Inorganic Chemistry, University of Cologne, Greinstr. 6, D-50859 Cologne, Germany.*

[b] *Department of Chemistry, Padova University and INSTM, Via Marzolo 1, 35131 Padova, Italy.*

[c] *Catalonia Institute for Energy Research (IREC), Barcelona, Spain.*

[d] *Multiscale Materials Modelling and Tribo Simulation, Fraunhofer IWM, Woehlerstr.11, 79108 Freiburg, Germany.*

[e] *Institute of Physical Chemistry, University of Cologne, Luxemburger Str.116, D-50939 Cologne, Germany.*

[f] *CNR-IENI and INSTM c/o Department of Chemistry, Padova University, Via Marzolo 1, 35151 Padova, Italy.*

[g] *Department of Chemistry and Bioengineering, Tampere University of Technology, P.O. Box 541 FI-33101 Tampere, Finland.*

KEYWORDS: Black Titania, Plasma Treatment, Photoelectrochemical Properties, Electrospinning.

Abstract

This work encompasses a facile method for tailoring surface defects in electrospun TiO_2 nanofibres by employing hydrogen plasma treatments. This amiable processing method was proven with SQUID, EPR, and XPS to be highly effective in generating oxygen vacancies, accompanied by the reduction of Ti^{4+} centres to Ti^{3+}, resulting in the formation of black titania. The treatment temperature was found to affect the Ti^{3+}/Ti^{4+} ratios and surface valence, while preserving the original 1D morphology of the titania fibres. *Ab initio* DFT calculations showed that a high concentration of oxygen vacancies is highly efficient in producing midgap states that enhance the system absorption over the whole visible range, as observed with UV/Vis/NIR diffuse reflectance spectroscopy. Pristine TiO_2 nanofibres produced a photocurrent density of ~0.02 mA/cm^2 at 1.23 V *vs.* RHE, whereas the hydrogen plasma treatment resulted in up to a ten-fold increase in the photoelectrochemical performance.

1) Introduction

During the last decade, solar-assisted water splitting has received considerable attention for the sustainable production of hydrogen, an attractive eco-friendly energy vector, from largely abundant and renewable resources. [1-9]

Among the various water oxidation catalysts, TiO_2 has been one of the most extensively studied semiconductors, since the pioneering work of Fujishima and Honda in 1972. [10] Nevertheless, the large band gap (3.2 eV) of TiO_2 limits its absorption especially in the visible part (400-800 nm)

of the solar spectrum, which represents a bottleneck for its large-scale utilization. [11] This intrinsic limitation has been addressed in a large body of data related to structural (core-shell, multi-layer, composite) and electronic (doped, co-doped, composite) modifications of titania. Tailoring and nano-engineering of TiO_2 systems has been investigated by modification of both fabrication routes and *ex-situ* treatments of titania-based compositions. [12] To this aim, various efforts have been devoted to chemically functionalize titania by incorporation of metal [13] or non-metal [14] entities. Approaches based on the surface modification of TiO_2 pigments by high pressure hydrogen treatment resulted in black titania powder.[15-16] Although the exact nature of the occurring chemical modification is not completely understood, the formation of midgap states above the valence band maximum is likely responsible for the creation of Ti^{3+} centres within the TiO_2 lattice, thus darkening the color of TiO_2 by modifying the band gap, which is of key importance for photocatalytic processes.[15, 17-18] So far black TiO_2 containing Ti^{3+} centres have been often accomplished by creating surface defects on the TiO_2 nano-particles/-rods under high pressure and extended reaction periods. [15-16] Particular attention was devoted to the use of milder conditions and shorter processing time with respect to previous reports showing that hydrogen plasma treatment is effective in improving functional performance of hematite photoanodes. [19]

Among the possible nanomaterial synthetic strategies, electrospinning is a very versatile approach for fabricating continuous and interwoven fiber networks with high active surface areas. One dimensional microstructure and reduced grain boundary regions ensure an efficient charge carrier transfer during photo-activated processes. [20-22] In this study, we have fabricated free-standing electrospun 1-D TiO_2 nanofibres and adopted hydrogen plasma treatments for the partial conversion of pristine TiO_2 to black titania.

2) Experimental Section

TiO_2 nanofibres were produced *via* the electrospinning of Ti sols (Figure 1a). [23] Typically, a solution of 1.4 g of Ti(IV) tetra-*iso*-propoxide ($Ti(O^iPr)_4$) in 5.0 mL of *iso*-propanol was mixed under vigorous stirring, followed by 0.318 mg acetic acid and 300 mg of polyvinylpyrrolidone (PVP, 1300000 g/mol) as the spinning-aid. As-obtained electrospun nanofibers were subjected to *ex-situ* annealing at 500 °C for 5 h to obtain a crystalline phase. The surface reduction was carried out using a Radio Frequency (RF)-plasma system (Domino CVD/PE-CVD, Plasma electronic), with a gas flow rate of 500 sccm, power 15 W and purity of 99,99 % in the temperature range 300-500° C for 3 h. The treatment of the target materials under hydrogen plasma resulted in a darkening of the initially white fibres, giving rise to black TiO_2, as shown in Figure 1b.

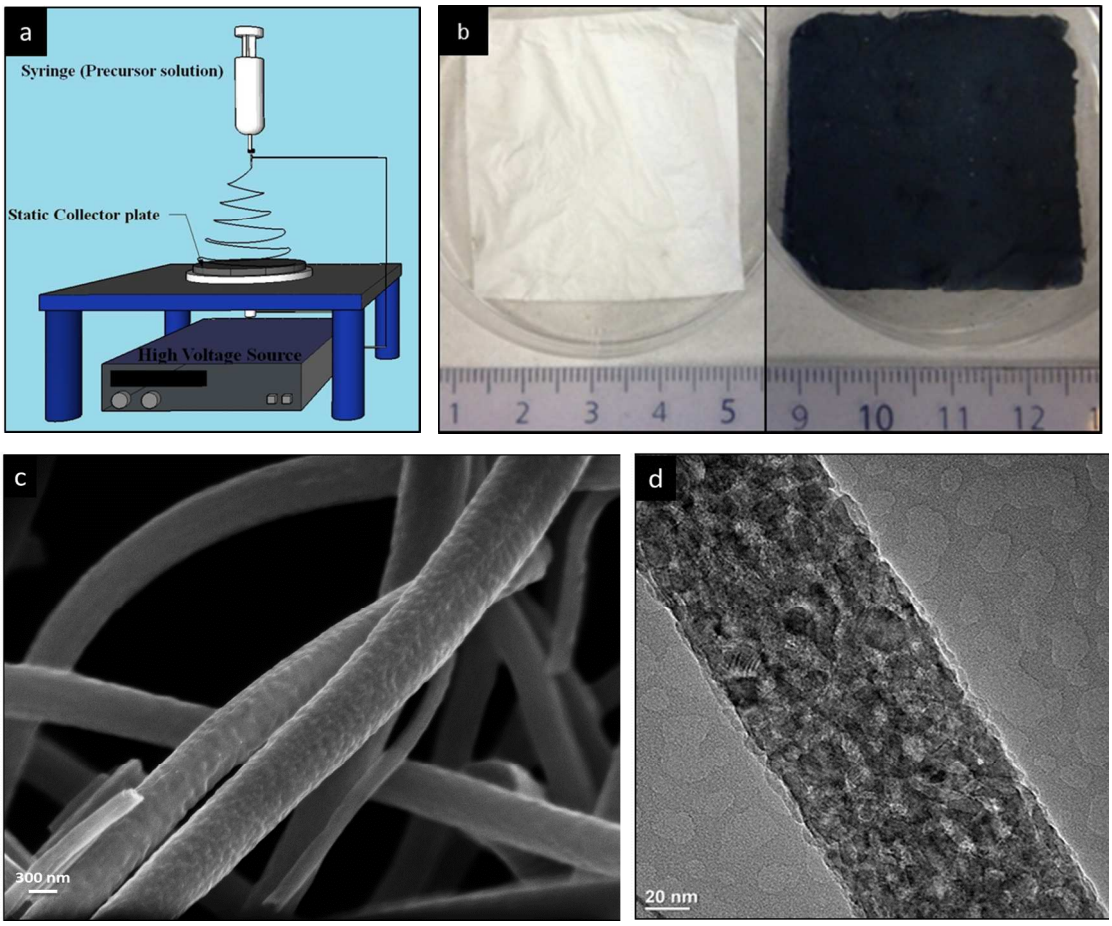

Figure 1 (a) Representative diagram showing an electrospinning process. (b) Optical difference between a pristine TiO_2 nanofibers (white) and hydrogen plasma treated fibres (black). (c) FE-SEM- and (d) HR-TEM- of the untreated TiO_2 nanofibres.

X-ray photoelectron spectroscopy (XPS) characterizations were conducted on a custom designed UHV system using Mg K_α excitation at a photon energy of 1253.6 eV and a Specs 100 hemispherical analyzer at 10 eV pass energy. The base pressure of the system is $3 \cdot 10^{-10}$ bar. The fitting of the XPS spectra was done using the program XPSPEAK Version 4.1. The concentration of the detected Ti^{3+} and Ti^{2+} species in relation to Ti^{4+} were calulated using the relative areas of their $2p_{3/2}$ peaks. UV

All PEC measurements were performed in a three-electrode electrochemical cell to obtain current-voltage (I-V) characteristics of the hydrogen plasma treated nanofibres and of the untreated pristine TiO_2 fibres. The fibrous networks were fabricated as electrodes by attaching the electrospun and annealed nanofibres to titanium gel covered FTO glass substrates (FTO-TEC, Sigma-Aldrich, ~8 Ω/sq) and heating to 500 °C for two hours, after which the electrodes were hydrogen plasma treated. Exposed FTO on the electrodes was connected to a silver wire with silver paste and covered with an epoxy resin. The electrodes had a well defined active surface area of 0.5 cm^2 and were employed as the working electrode under dark and illuminated conditions with a 150 W Xenon lamp (Newport, Model: 67005) and an AM 1.5G filter. 1M NaOH electrolyte (pH = 13.6) was used as the electrolyte to record I-V characteristics at varying applied potentials from +0.8 V/SCE (anodic bias) to -0.8 V/SCE (cathodic bias) with a scan rate

of 10 mV/s for all samples. The applied potentials versus SCE were calculated versus the reversible hydrogen electrode (RHE) using the following equation: [19]

$$E_{RHE} = E_{SCE} + E^0_{SCE} + 0.059pH$$

The photocurrent density was calculated from the linear-sweep voltammograms under dark and illumination conditions and plotted as a function of applied potential.

3) Results and Discussion

Field Emission-Scanning Electron Microscopy (FE-SEM) and High Resolution-Transmission Electron Microscopy (HR-TEM) micrographs (Figures 1c and 1d) revealed the spatial organization of highly interwoven nanofibres with diameter ~400 nm. The performed plasma treatment did not induce any appreciable variation in the morphology of the fibres such as increased roughness, cleavage, peeling or branching phenomena [Figures 3–6 in the Electronic Supplementary Information (ESI)]. Irrespective of the adopted synthesis and plasma-treatment conditions, X-ray diffraction (XRD) indicated the formation of the *anatase* phase (Figure 2a; JCPDS Card: 78-2486), free from other possible titania polymorphs. A careful inspection of the XRD results show a decrease in the peak intensity upon increasing the hydrogen plasma treatment temperature. This phenomenon, particularly evident for the (101) reflection, could be related to the formation of atomistic surface defects that do not cause any extensive surface roughening, since the plasma power used in our treatment is lower than that required for

etching. [24-25] Nevertheless, the bombardment of the target nanomaterials by hydrogen ions with high kinetic energy produces surface vacancies by removing oxygen species, thus increasing the structural disorder of the nanofiber surfaces. [26] In addition, the chemical composition of the nanofibres can change due to the incorporation of hydrogen into the TiO_2 lattice to form gradient (TiO_2@$TiO_{2-x}H_x$) structures with reduced Ti centers [Ti(IV) → Ti(III)].

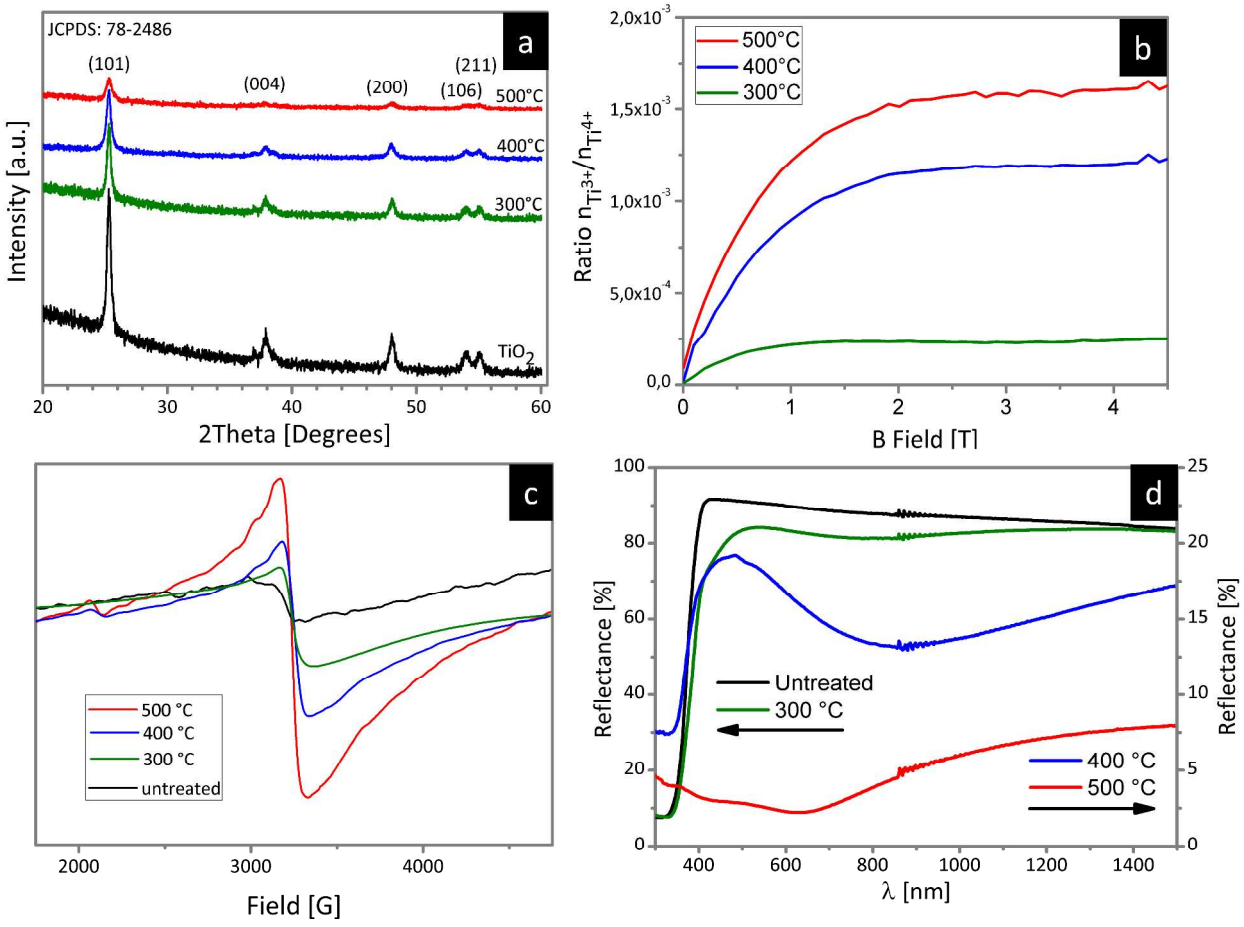

Figure 2 (a) XRD patterns of the untreated TiO_2 and H_2 plasma treated TiO_2 nanofibres different plasma treatment temperatures (b) SQUID measurements of H_2 plasma treated TiO_2 samples performed at 2 K. (c) EPR measurements of the pure TiO_2 and H_2 plasma treated TiO_2 . (d) UV/Vis/NIR reflectance spectra of the untreated and H_2 plasma treated TiO_2 samples.

In order to attain a deeper insight into the mentioned phenomena, particularly regarding the formation of oxygen vacancies upon hydrogen plasma treatment, magnetic measurements were carried out. Whereas pure anatase TiO_2 is diamagnetic, the partial reduction of Ti^{4+} centers to Ti^{3+} upon formation of oxygen defects leads to paramagnetic behavior. SQUID measurements of the plasma treated samples clearly showed that an increase in the processing temperature corresponded with an overall increment in the content of paramagnetic species in the fiber surfaces (Figure 2b). This evidences that H_2 plasma treatment induces the formation of oxygen vacancies and the partial reduction of the neighbouring Ti^{4+} centers to Ti^{3+}, a phenomenon further promoted by an increased processing temperature. [26]

To corroborate the presence of paramagnetic Ti^{3+} centers in the target systems and to substantiate the magnetic measurements, Electron Paramagnetic Resonance (EPR) spectroscopy was performed. In particular, X-Band EPR-spectra recorded before and after H_2 plasma treatment of TiO_2 fibres exhibited EPR signals for all samples. The low intensity signals with *g*-values of 1.982 G are assigned to Ti^{3+}species. [27] Figure 2c shows the EPR-spectrum of the TiO_2 fibres H_2 plasma treated at 500 °C,400°C and 300°C compared to that of untreated TiO_2. The signal intensity significantly increased upon hydrogen plasma treatment when compared to the untreated sample. The EPR results suggest that the electrons are located in the d-orbitals. Thus, J = S = ½ is a fair approximation for the electrons, and the saturation moment for each Ti^{3+} equals 1 μB. Hence, the saturation moment for each curve represents the relative amount of Ti^{3+} in a diamagnetic matrix. [28]

Optical reflectance spectra versus a Spectralon reference were measured in the UV (300 nm) to near IR (1500 nm) region as seen in Figure 2d. The untreated TiO_2 fibres have no absorption in the visible and near infrared regions with the band gap absorption beginning at 405 nm (optical

band gap ~3.1 eV). The H_2 plasma treatment has a drastic effect on the sample absorption as indicated by the observed gradual color change to black. The plasma treatment at 300 °C results in a broad but low intensity absorbance around 800 nm and a redshift of the band gap absorption to 450 nm. Plasma treatment at higher temperatures results in a noticeably lowered reflectance in the whole measurement range. The broad absorption band has a maximum at 860 nm on the 400 °C plasma treated sample, while the band gap absorption remains practically unchanged from the 300 °C plasma treated sample. On the other hand, no TiO_2 specific band gap absorption is observed anymore for the 500 °C plasma treated sample. The increased absorption of this sample has a maximum at 630 nm due to localised empty midgap states lying ~2.0 eV above the valence band level that coincides with the previously reported band gap of black TiO_2.[15] Therefore, from the diffuse reflectance data we deduce that the lack of a TiO_2 specific band gap absorption in the UV range suggests a saturation of the defects on the surface of the nanofibres, which is further supported by the drop in the XRD peak intensity (Figure 2a).

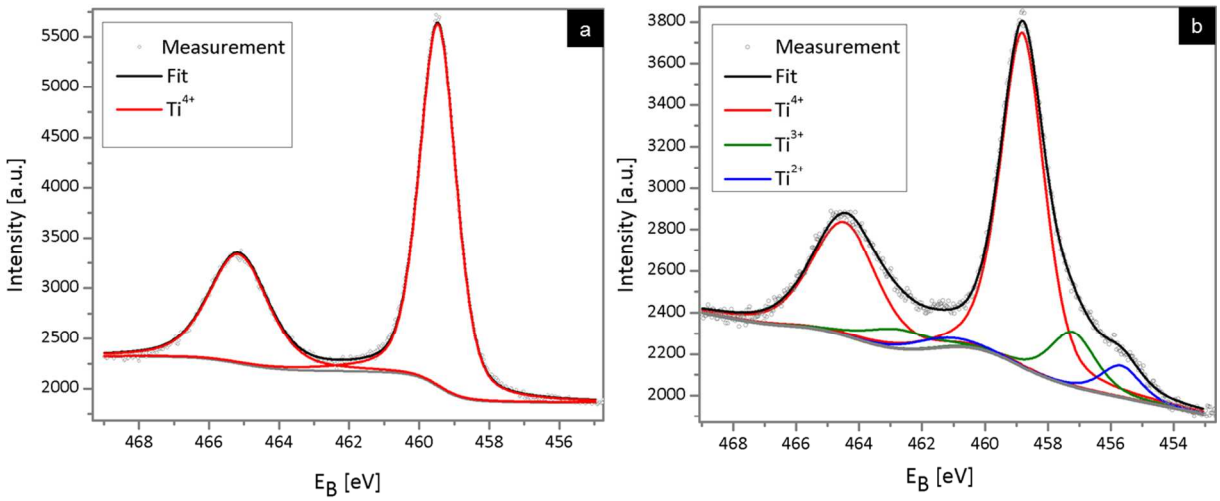

Figure. 3 XPS spectra Ti 2*p* core level peaks for: (a) untreated TiO_2 and (b) hydrogen plasma treated TiO_2 samples at 500°C.

Figure 3a displays the XPS spectra for the Ti 2*p* core level of nanofibres before hydrogen plasma treatment. The spin orbit splitting between the two p peaks is 5.7 eV and the intensity ratio is 2:1, as expected. The $2p_{3/2}$ component can be well fitted with a single peak, centered at a binding energy (BE) of 459.5 eV, having a full width at half maximum (FWHM) of 1.24 eV. These values are characteristic for octahedral Ti^{4+} in TiO_2. [29-30] In contrast, hydrogen plasma treated fibres at 500°C (Figure 3b) show a change in the spectrum shape, with the appearance of low-BE shoulders that suggest the co-presence of Ti oxidation states lower than 4. Spectral deconvolution showed the presence of two additional bands with BEs of 457.20 eV and 455.68 eV (FWHM = 1.71 and 1.49 eV, respectively) which can be attributed to $2p_{3/2}$ peaks of Ti^{3+} and Ti^{2+}. [31-32] The creation of Ti^{2+} species could be a direct result of the high degree of reduction during the hydrogen plasma treatment. [33] The relative amounts of Ti^{3+} and Ti^{2+} formed as a result of the valence electron transition compared with Ti^{4+} were 13.5% and 6.8%, respectively. XPS spectra for samples treated with hydrogen plasma at 300°C and 400°C do not show additional oxidation states other than Ti^{4+}, despite a continuous peak broadening with the increase in the hydrogen plasma treatment temperatures (Figure 8 in the ESI).

Ab-initio calculations within the GGA+U framework of density functional theory (DFT) have been used in order to investigate the influence of oxygen vacancies on the electronic structure of anatase TiO_2. [34-36] A direct comparison to the effect of lattice disorder as proposed by Chen *et. al* is made. [10] A special focus is put on the effect of disorder in the crystal structure. Our results indicate that a mild hydrogen treatment process that leaves the crystal structure intact is favourable compared to hydrogen treatment processes that generate highly disordered TiO_2 lattices.

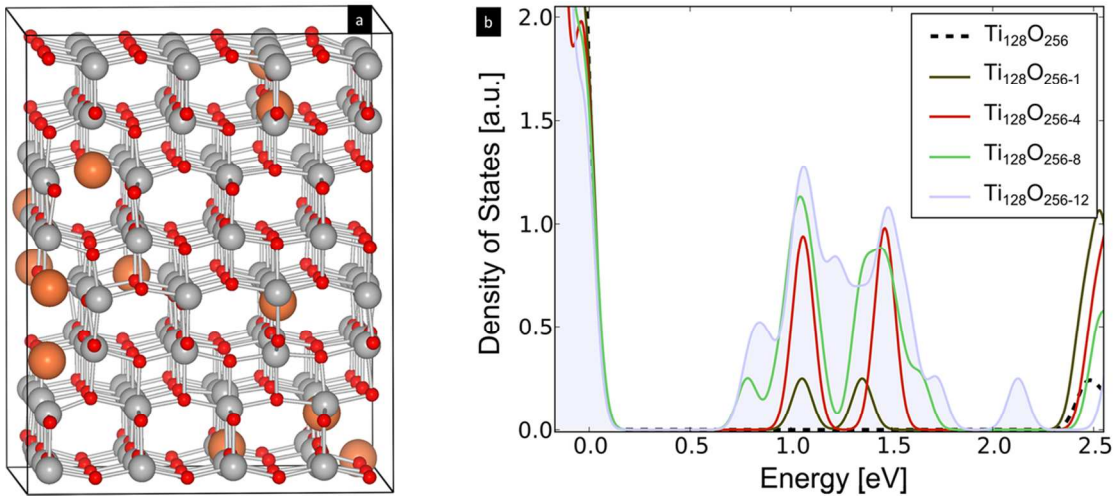

Figure 4 a) Anatase TiO_2 supercell with the composition $Ti_{128}O_{256-12}$. The 12 oxygen vacancies on random positions in the anatase cell are shown as large brownish spheres. Ti ions are shown in grey and oxygen ions in red. b) Density of electronic states (DoS) of TiO_2 for varying oxygen vacancy concentrations. Occupied energy levels are indicated by the shaded areas. With increasing oxygen vacancy concentrations the spectrum of midgap states formed by localized Ti^{3+} centers broadens.

In the first step, oxygen vacancies were generated with different concentrations in random sites in the TiO_2 lattice, shown in Figure 4a. The density of states (DoS) for the different configurations was calculated after a full relaxation of the employed supercells with the compositions $Ti_{128}O_{256-x}$, x=0, 1, 4, 8, 12 and is shown in Figure 4b. Below oxygen vacancy concentrations of 0.9 nm^{-3}, *i.e.* for the supercell $Ti_{128}O_{256-4}$, the DoS reveals two distinct peaks of occupied electronic states, which are localized at different Ti^{3+} centers near the defect sites. This is in agreement with previous work where single oxygen vacancies were investigated.[36] Upon increasing the defect concentration, the two peaks broaden considerably and finally merge, yielding a broad spectrum of midgap states. These results indicate that a rather high

concentration of oxygen vacancies (~1–2 nm^{-3}) is needed in order to enhance the absorption of TiO_2 over a broad photon spectrum, supporting the conclusion from DRS data that the surface defecct density is possibly saturated for the sample treated at 500 °C.

The SQUID measurements show that the concentrations of Ti^{3+} centers in the overall hydrogenated samples are rather small (see Figure 2b). This suggests that in our experiments oxygen vacancies are mainly formed within a small region near the surface of the nanofibres, due to the limited plasma penetration into the TiO_2 nanofibres. [37] This is consistent with the enhanced values of the Ti^{3+}/Ti^{4+} ratio for our hydrogen treated samples in the surface sensitive XPS measurements.

The TiO_2 (001) surface is usually considered to be catalytically more active for oxygen evolution reactions. [38] Subsequently, the electronic structure of the (001) TiO_2 surface in the presence of oxygen vacancies was simulated, investigating also the effect of lattice disorders, including hydrogen interstitials. [16]

To this aim, we employed TiO_2 *anatase* slabs (thickness 2.8 nm) terminated by (001) surfaces and periodically repeated in the transverse directions. Whereas the lower half of the slabs were unmodified, 6 oxygen vacancies and 12 interstitial hydrogens were incorporated in the upper half of the unit cell with composition $Ti_{108}O_{216}$ (Figure 5a), corresponding to impurity concentrations of 3.1 nm^{-3} and 6.2 nm^{-3}, respectively. Since an interstitial hydrogen impurity donates one electron and a single oxygen vacancy creates two Ti^{3+} states, the same amount of Ti^{3+} states are generated in the two cases. The hydrogenated slab was additionally annealed to 3000K for 2 ps and subsequently fully relaxed. The atoms in the lower half of the slab were kept fixed. In this way the model for a disordered surface structure shown in Figure 5a was obtained.

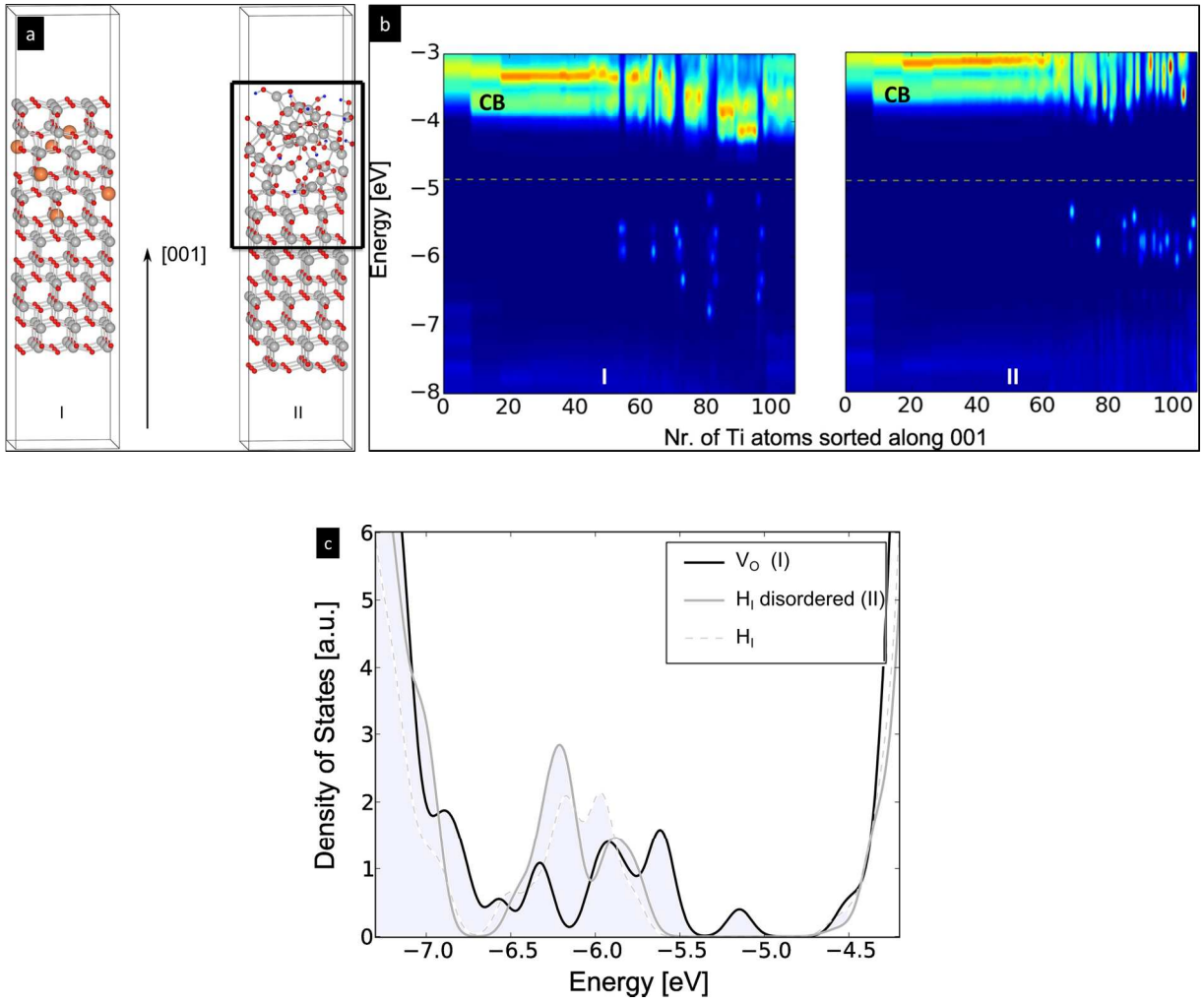

Figure 5 (a) TiO_2 slab with an oxygen vacancy concentration of approximately 3.1 nm^{-3} (I) and a disordered crystal structure with hydrogen interstitial concentration of 6.2 nm^{-3} (II) in the upper half within the black frame. (b) DoS projected on the Ti atoms for the simulated slab configurations I and II with oxygen vacancies and interstitial hydrogen atoms in a disordered lattice. The Fermi level is indicated by the yellow dashed lines. The Ti orbitals mainly form the midgap states as well as the conduction band (CB). (c) Densities of states (DoS) of the surface configurations I with oxygen vacancies (V_O) and II with a disordered crystal structure and interstitial H atoms (H_I disordered). Additionally, the DoS of interstitial H atoms in an ordered crystal structure (H_I) is depicted. The shown DoS is obtained by a summation of the atom

projected DoS of the atoms in the upper half of the slabs. Occupied energy levels are indicated by the shaded areas. The vacuum potential is taken as the zero energy reference.

In both cases, the atom projected density of states (PDoS) was calculated. The PDoS confirms that midgap states are introduced by both oxygen vacancies and hydrogen intertitials, with the states being occupied and located at the Ti sites, see Figure 5b. Hence, the formation of Ti^{3+} centres, as observed by XPS analyses, is substantiated. However, in the case of oxygen vacancies, the energy spectrum of the midgap states is considerably broader for identical Ti^{3+} concentrations. From the PDoS we also find that the disordered crystal structure of the annealed sample lead to a highly fluctuating energy spectrum at the conduction band edges as shown in Figure 5b. The same behavior is also found at the valence band edges (not shown). This indicates the formation of localized states at the band edges, which likely act as traps for electrons and holes, respectively. On the other hand, the incorporation of oxygen vacancies into the ordered crystal structure leaves the energy spectrum at the band edges relatively smooth, and therefore indicates superior transport properties compared to the disordered hydrogenated system.

The finding that the midgap states show higher peaks for the hydrogenated disordered sample, while the configuration with the oxygen vacancies shows a broader level distribution, is also verified by analysing the sum of the densities of states projected on the atoms of the upper half of the slabs (Figure 5c).

The density of states of a configuration with interstitial hydrogen defects in an ordered TiO_2 crystal structure was also investigated. Here we again observe a rather narrow distribution of midgap states. However, at the hydrogen interstitial concentration of 6.2 nm^{-3}, we find that the occupation of states at the conduction band minimum indicates that at such high hydrogen doping levels delocalized charge carriers are generated, leading to enhanced conductivity of the

TiO_2. Since the improvement of the electrical transport properties is considered as one of the major issues that have to be addressed for highly efficient metal oxide photoelectrodes, [39] the incorporation of a high concentration of hydrogen interstitials into the ordered *anatase* lattice may lead to enhanced photoelectrochemical performance.

The performed simulations indicate that compared with hydrogen interstitials the oxygen vacancies are highly efficient in generating a broad spectrum of midgap states, enhancing light absorption over a broad photon spectrum. This finding explains why a relatively mild plasma treatment that generates oxygen vacancies is sufficient for the fabrication of black TiO_2, which maintains its crystal structure intact, a very attractive aspect concerning the mobility of charge carriers. We also observe a strong localization of states in the disordered slab configuration with interstitial hydrogen atoms, which can explain a significant drop of charge carrier mobility in disordered TiO_2 lattices. [40]

In order to elucidate the photoactivity of the nanofibres, photoelectrochemical measurements (PEC) were carried out, shown in Figure 6. We observe a gradual increase in the photocurrent density (j) at 1.23 V *vs*. RHE from ~0.02 mA/cm^2 for the pristine TiO_2 to a maximum of ~0.2 mA/cm^2 for the TiO_2 nanofibres H_2 plasma treated at 500°C. This indicates a tenfold increase in the photoelectrochemical performance due to the increased absorption of the fibres. The fact that photocurrent densities increase gradually with higher treatment temperatures indicates clearly that the process temperature assists the reduction of the TiO_2 nanofibres. In addition, an increase in the treatment temperature resulted in a cathodic shift of the photocurrrent onset voltage. This shift illustrates a reduction of the applied bias that is required to produce photocurrent, enhancing the photoelectrochemical performance of the working electrode. The growth of the photocurrent is linear for the pristine TiO_2 after ~0.6 V *vs*. RHE, whereas this

value is lowered to 0.3 V (300°C), 0.25 V (400°C) and 0.2 V (500°C) *vs*. RHE for the H_2 plasma treated fibres. The rapid increase in the photocurrent densities at lower potentials demonstrates improved charge separation and transport of charge carriers. These enhancements due to hydrogen plasma treatment under mild conditions, combined with the outcomes of theoretical simulations clearly demonstrate that an improvement in the overall PEC performance occurs due to the creation of oxygen vacancies. When compared with existing data on 0–2 dimensional TiO_2 nanostructures, photocurrent densities achieved in this study are relatively modest.[41] This discrepancy can be explained by the sparse contact at the interface between the conducting glass and the nanofibres, hindering efficient transfer of photogenerated carriers and producing at least a partial recombination. This is clearly observed for the untreated fibres as well. Further work to circumvent this problem is already in progress.

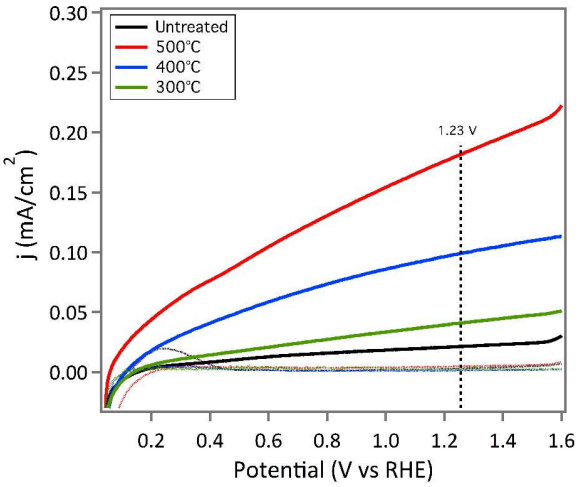

Figure 6 Photocurrent density *vs*. applied potential curves for *titania* nanofibres treated under different conditions. Dotted and solid lines represent the measurements in the dark and under illumination, respectively. For clarity, the j values at 1.23 V *vs*. RHE *i.e* at the theoretical water oxidation potential, are marked by a dashed line.

Conclusions

In summary, this work presented a facile route for tailoring the surface defects in TiO_2 nanostructures fabricated by electrospinning by employing mild hydrogen plasma treatments. The adopted modification process was proven to be effective in generating oxygen vacancies in TiO_2, accompanied by the reduction of Ti^{4+} centres to Ti^{3+}. Variations in the treatment temperatures were observed to be able to finely modulate the Ti^{3+}/Ti^{4+} ratios and valence dynamics on the surface, while preserving the original one dimensional morphology of the titania nanofibres. Computational studies demonstrated that a high concentration of oxygen vacancies resulted in a broad spectrum of midgap states that enhanced the system absorption over the visible range. The increased absorption resulted in greatly enhanced PEC performances. However, the introduction of disorder in the TiO_2 lattice was identified to be detrimental for the electronic transport properties. Interestingly, this could be tailored as a function of the temperature adopted during the plasma processing. These results disclose attractive perspectives for the engineering of photoelectrochemical systems that could be adapted to a broad range of usages.

ASSOCIATED CONTENT:

Supporting Information

Detailed procedures for the fabrication of TiO_2 nanofibres, hydrogen plasma treatment and characterization such as EDXS Mapping and HR-TEM are included in the Supporting Information.

AUTHOR INFORMATION

Corresponding Author:

* *Email:* sanjay.mathur@uni-koeln.de Tel:+4922147015627

ACKNOWLEDGMENT

We gratefully acknowledge the University of Cologne and SOLAROGENIX Project (EC-FP7-Grant Agreement No. 310333) for the financial support. C. Maccato and D. Barreca kindly acknowledge the financial support under the Padova University ex-60% 2012-2014 and INSTM-Regione Lombardia ATLANTE grants. Thanks are due to Dr. Christian Biewer, Katrin Stirnat and Dr. Martin Valldor from the University of Cologne for their help in EPR and SQUID measurements and to Dr. Yakup Gonüllü and Thomas Fischer, University of Cologne for their scientific feed-back.

REFERENCES

(1) Mettee, H. D., Solar-Induced Water Splitting. *Chem Eng News* **1989**, *67*, 3-3.

(2) Vayssieres, L., All-Oxide Heteronanostructures for Solar Water Splitting. *Abstr Pap Am Chem S* **2012**, *244*.

(3) Xiao, L.; Wu, S. Y.; Li, Y. R., Advances in Solar Hydrogen Production Via Two-Step Water-Splitting Thermochemical Cycles Based on Metal Redox Reactions. *Renew Energ* **2012**, *41*, 1-12.

(4) Barreca, D.; Carraro, G.; Gasparotto, A.; Maccato, C.; Sada, C.; Singh, A. P.; Mathur, S.; Mettenborger, A.; Bontempi, E.; Depero, L. E., Columnar Fe_2O_3 Arrays Via Plasma-Enhanced Growth: Interplay of Fluorine Substitution and Photoelectrochemical Properties. *Int J Hydrogen Energ* **2013**, *38*, 14189-14199.

(5) Liao, L. B., et al., Efficient Solar Water-Splitting Using a Nanocrystalline Coo Photocatalyst. *Nat Nanotechnol* **2014**, *9*, 69-73.

(6) Mubeen, S.; Lee, J.; Singh, N.; Kramer, S.; Stucky, G. D.; Moskovits, M., An Autonomous Photosynthetic Device in Which All Charge Carriers Derive from Surface Plasmons. *Nat Nano* **2013**, *8*, 247-251.

(7) Abdi, F. F.; Han, L.; Smets, A. H. M.; Zeman, M.; Dam, B.; van de Krol, R., Efficient Solar Water Splitting by Enhanced Charge Separation in a Bismuth Vanadate-Silicon Tandem Photoelectrode. *Nat Commun* **2013**, *4*.

(8) Liu, B.; Wu, C. H.; Miao, J. W.; Yang, P. D., All Inorganic Semiconductor Nanowire Mesh for Direct Solar Water Splitting. *Acs Nano* **2014**, *8*, 11739-11744.

(9) Warren, S. C.; Voïtchovsky, K.; Dotan, H.; Leroy, C. M.; Cornuz, M.; Stellacci, F.; Hébert, C.; Rothschild, A.; Grätzel, M., Identifying Champion Nanostructures for Solar Water-Splitting. *Nat Mater* **2013**, *12*, 842-849.

(10) Fujishima, A.; Honda, K., Electrochemical Photolysis of Water at a Semiconductor Electrode. *Nature* **1972**, *238*, 37-38.

(11) Kudo, A.; Omori, K.; Kato, H., A Novel Aqueous Process for Preparation of Crystal Form-Controlled and Highly Crystalline $BiVO_4$ Powder from Layered Vanadates at Room Temperature and Its Photocatalytic and Photophysical Properties. *J Am Chem Soc* **1999**, *121*, 11459-11467.

(12) Li, Z. S.; Luo, W. J.; Zhang, M. L.; Feng, J. Y.; Zou, Z. G., Photoelectrochemical Cells for Solar Hydrogen Production: Current State of Promising Photoelectrodes, Methods to Improve Their Properties, and Outlook. *Energ Environ Sci* **2013**, *6*, 347-370.

(13) Choi, W.; Termin, A.; Hoffmann, M. R., Einflüsse Von Dotierungs-Metall-Ionen Auf Die Photokatalytische Reaktivität Von TiO_2-Quantenteilchen. *Angewandte Chemie* **1994**, *106*, 1148-1149.

(14) Chen, X.; Burda, C., Photoelectron Spectroscopic Investigation of Nitrogen-Doped Titania Nanoparticles. *The Journal of Physical Chemistry B* **2004**, *108*, 15446-15449.

(15) Chen, X. B.; Liu, L.; Yu, P. Y.; Mao, S. S., Increasing Solar Absorption for Photocatalysis with Black Hydrogenated Titanium Dioxide Nanocrystals. *Science* **2011**, *331*, 746-750.

(16) Chen, X. B., et al., Properties of Disorder-Engineered Black Titanium Dioxide Nanoparticles through Hydrogenation. *Sci Rep-Uk* **2013**, *3*.
(17) Wang, G.; Wang, H.; Ling, Y.; Tang, Y.; Yang, X.; Fitzmorris, R. C.; Wang, C.; Zhang, J. Z.; Li, Y., Hydrogen-Treated TiO_2 Nanowire Arrays for Photoelectrochemical Water Splitting. *Nano Lett* **2011**, *11*, 3026-3033.
(18) Islam, M. M.; Calatayud, M.; Pacchioni, G., Hydrogen Adsorption and Diffusion on the Anatase TiO_2(101) Surface: A First-Principles Investigation. *The Journal of Physical Chemistry C* **2011**, *115*, 6809-6814.
(19) Mettenbörger, A.; Singh, T.; Singh, A. P.; Järvi, T. T.; Moseler, M.; Valldor, M.; Mathur, S., Plasma-Chemical Reduction of Iron Oxide Photoanodes for Efficient Solar Hydrogen Production. *Int J Hydrogen Energ* **2014**, *39*, 4828-4835.
(20) Li, L. L.; Peng, S. J.; Wang, J.; Cheah, Y. L.; Teh, P. F.; Ko, Y. W.; Wong, C. L.; Srinivasan, M., Facile Approach to Prepare Porous Casno3 Nanotubes Via a Single Spinneret Electrospinning Technique as Anodes for Lithium Ion Batteries. *Acs Appl Mater Inter* **2012**, *4*, 6005-6012.
(21) Li, D.; Xia, Y., Electrospinning of Nanofibers: Reinventing the Wheel? *Advanced Materials* **2004**, *16*, 1151-1170.
(22) Cavaliere, S.; Subianto, S.; Savych, I.; Jones, D. J.; Roziere, J., Electrospinning: Designed Architectures for Energy Conversion and Storage Devices. *Energ Environ Sci* **2011**, *4*, 4761-4785.
(23) Formo, E.; Lee, E.; Campbell, D.; Xia, Y., Functionalization of Electrospun TiO_2 Nanofibers with Pt Nanoparticles and Nanowires for Catalytic Applications. *Nano Lett* **2008**, *8*, 668-672.
(24) Hotovy, I.; Hascik, S.; Gregor, M.; Rehacek, V.; Predanocy, M.; Plecenik, A., Dry Etching Characteristics of TiO_2 Thin Films Using Inductively Coupled Plasma for Gas Sensing. *Vacuum* **2014**, *107*, 20-22.
(25) Mathur, S.; Ganesan, R.; Grobelsek, I.; Shen, H.; Ruegamer, T.; Barth, S., Plasma-Assisted Modulation of Morphology and Composition in Tin Oxide Nanostructures for Sensing Applications. *Adv Eng Mater* **2007**, *9*, 658-663.
(26) Pan, J.; Ganesan, R.; Shen, H.; Mathur, S., Plasma-Modified SnO_2 Nanowires for Enhanced Gas Sensing. *J Phys Chem C* **2010**, *114*, 8245-8250.
(27) Xiong, L. B.; Li, J. L.; Yang, B.; Yu, Y., Ti^{3+} in the Surface of Titanium Dioxide: Generation, Properties and Photocatalytic Application. *J Nanomater* **2012**.
(28) Goodman, B. A.; Raynor, J. B., Electron Spin Resonance of Transition Metal Complexes. In *Advances in Inorganic Chemistry and Radiochemistry*, Emeléus, H. J.; Sharpe, A. G., Eds. Academic Press: 1970; Vol. Volume 13, pp 135-362.
(29) Ruzicka, J.-Y.; Bakar, F. A.; Thomsen, L.; Cowie, B. C.; McNicoll, C.; Kemmitt, T.; Brand, H. E. A.; Ingham, B.; Andersson, G. G.; Golovko, V. B., Xps and Nexafs Study of Fluorine Modified TiO_2 Nano-Ovoids Reveals Dependence of Ti^{3+} Surface Population on the Modifying Agent. *Rsc Adv* **2014**, *4*, 20649-20658.
(30) Yang, K. Y.; Fung, K. Z.; Wang, M. C., X-Ray Photoelectron Spectroscopic and Secondary Ion Mass Spectroscopic Examinations of Metallic-Lithium-Activated Donor Doping Process on $La_{0.56}Li_{0.33}TiO_3$ Surface at Room Temperature. *J Appl Phys* **2006**, *100*.
(31) Guillemot, F.; Porte, M. C.; Labrugere, C.; Baquey, C., Ti^{4+} to Ti^{3+} Conversion of TiO_2 Uppermost Layer by Low-Temperature Vacuum Annealing: Interest for Titanium Biomedical Applications. *J Colloid Interf Sci* **2002**, *255*, 75-78.

(32) Wang, L. Q.; Baer, D. R.; Engelhard, M. H., Creation of Variable Concentrations of Defects on TiO_2,(110) Using Low-Density Electron-Beams. *Surf Sci* **1994**, *320*, 295-306.
(33) Gopel, W.; Anderson, J. A.; Frankel, D.; Jaehnig, M.; Phillips, K.; Schafer, J. A.; Rocker, G., Surface-Defects of TiO_2(110) - a Combined Xps, Xaes and Els Study. *Surf Sci* **1984**, *139*, 333-346.
(34) Anisimov, V. I.; Zaanen, J.; Andersen, O. K., Band Theory and Mott Insulators - Hubbard-U Instead of Stoner-I. *Phys Rev B* **1991**, *44*, 943-954.
(35) Liechtenstein, A. I.; Anisimov, V. I.; Zaanen, J., Density-Functional Theory and Strong-Interactions - Orbital Ordering in Mott-Hubbard Insulators. *Phys Rev B* **1995**, *52*, R5467-R5470.
(36) Finazzi, E.; Di Valentin, C.; Pacchioni, G.; Selloni, A., Excess Electron States in Reduced Bulk Anatase TiO(2): Comparison of Standard Gga, Gga Plus U, and Hybrid Dft Calculations. *J Chem Phys* **2008**, *129*.
(37) Pan, J.; Ganesan, R.; Shen, H.; Mathur, S., Plasma-Modified Sno2 Nanowires for Enhanced Gas Sensing. *The Journal of Physical Chemistry C* **2010**, *114*, 8245-8250.
(38) Roy, N.; Sohn, Y.; Pradhan, D., Synergy of Low-Energy {101} and High-Energy {001} TiO_2 Crystal Facets for Enhanced Photocatalysis. *Acs Nano* **2013**, *7*, 2532-2540.
(39) Sivula, K., Metal Oxide Photoelectrodes for Solar Fuel Production, Surface Traps, and Catalysis. *The Journal of Physical Chemistry Letters* **2013**, *4*, 1624-1633.
(40) Wu, N.; Wang, J.; Tafen, D. N.; Wang, H.; Zheng, J.-G.; Lewis, J. P.; Liu, X.; Leonard, S. S.; Manivannan, A., Shape-Enhanced Photocatalytic Activity of Single-Crystalline Anatase TiO_2 (101) Nanobelts. *J Am Chem Soc* **2010**, *132*, 6679-6685.
(41) Kusior, A.; Wnuk, A.; Trenczek-Zajac, A.; Zakrzewska, K.; Radecka, M., TiO_2 Nanostructures for Photoelectrochemical Cells (Pecs). *Int J Hydrogen Energ*. (*in Press*)